Modeling droplet phase change in the presence of a multi-component gas mixture

Damien Furfaro and Richard Saurel
Aix-Marseille University, 5 rue. E. Fermi, 13453 Marseille Cedex 13, France

Abstract

Dispersed liquid droplet flows with evaporation and condensation in multi-component gas mixture made of vapor and other gas phase chemical species such as air occur in many engineering applications dealing with two-phase flows. However, existing models are essentially derived for vaporization occurring in sprays combustion. It means that the energy is transferred from a hot gas to the liquid to produce its phase change. This is thus a non-symmetric approach as in some situations the energy is already stored in the liquid phase and flashing occurs as a consequence pressure drop.

In the present paper a droplet mass transfer model is derived and is valid in any situation: evaporation, flashing and condensation. It accounts for:

- coupled heat and mass diffusion in the gas phase,
- thermodynamics of the multi-component gas mixture,
- heat diffusion inside the liquid droplet, enabling consideration of both droplet heating and cooling. These effects are important in evaporating and flashing situations respectively.

The resulting model consists in an algebraic non-linear system of three equations giving the interface temperature, the mass flow rate and vapor species concentration at the interface. These interfacial variables enable computation of the mass species, momentum and energy transfer rates appearing in volume averaged two-phase flow models.

Computational examples are shown with this mass transfer model embedded in a compressible two-phase flow model of Baer and Nunziato (1986) type.

Keywords : Heat and mass transfers, Fick and Fourier laws, local and volume averaged models, two-phase flows, hyperbolic systems.

Corresponding author:
Tel: +339-72-45-86-94
Email addresses: Richard.Saurel@rs2n.com

1. Introduction

Dispersed droplet flows with phase change appear in many fundamental and applied science situations such as for example combustion in automotive and spacecraft engines, cryogenic combustion and atmospheric liquid dispersion to cite a few. In most situations phase change occurs between liquid drops and corresponding vapour mixed with other gas phase chemical species, such as for example air. In such instances, phase change involves both heat diffusion in the liquid and gas phases as well as mass diffusion of the chemical species in the gas phase.

Main difficulties related to such modelling are related to multidimensional effects that have to be summarized algebraically, i.e. in 0D. Many efforts have been carried out in this direction, mainly in the frame of two-phase spray combustion (Spalding, 1953, Williams, 1958, Law, 1982, Abramzon and Sirignano, 1989, Abramzon and Sazhin 2005, Sirignano, 2014, and references therein). In the last reference arrays of droplets were considered while in former ones isolated droplets only were studied.

The present work considers the behaviour of a single droplet, cumulative effects to the mean flow being accounted for through the specific interfacial area of the droplets cloud, under the assumption of absence of interaction between drops.

The present contribution follows the lines of Abramzon and Sirignano (1989) (AS89) in the sense that:

- Gas phase boundary layer effects around the droplet are considered through Nusselt and Sherwood numbers correlations. This method enables computation of heat and mass diffusion fluxes through the gas to the interface without spatial resolution of the surrounding gas. Also, this approach considers velocity slip between the liquid and gas phases as Sherwood and Nusselt numbers correlations account for it through the particle Reynolds number.
- Local thermodynamic equilibrium is considered at the interface.
- Droplet heating is considered through a heat exchange coefficient between the liquid-gas interface and the droplet core. In AS89 two-dimensional flow internal to the droplet was considered to this respect.

However, the AS89 model was derived in the aim of spray combustion modelling. In such a situation phase change occurs as a result of heat exchange from the (hot) gas to the (initially cold) droplet. The internal heat exchange to the droplet is needed to compute:

- droplet heating before reaching the saturation temperature,
- heat losses from the interface to the cold droplet core that lower the mass transfer rate through the interface energy balance.

In AS89 the energy exchange internal to the droplet is thus a corrective term to the main heat flux that comes from the gas to the interface.

In situations different to spray combustion the mass transfer rate may be a result of the energy already stored in the liquid droplet. Such situations occur for instance when the surrounding gas is suddenly depressurized, as for example in nozzle flows or in the whole sequence of spherical explosions. In these situations the liquid core temperature is higher than the saturation temperature at local pressure. Consequently droplet flashing occurs as a limit case.

In the present work a phase transition model valid in any situation is built as a generalisation and non-linear extension of the AS89 model. Both liquid and gas diffusion effects are considered without giving priority to the gas transfer heat exchange to the interface. In this sense, the model becomes symmetric and as a consequence, highly non-linear.

Rather than having weakly coupled relations for the mass and heat transfers terms such as in the AS89 model a fully coupled non-linear system of three algebraic equations is obtained. This is the first main difference. These algebraic equations are clearly established from local jump conditions

of mass and energy at the interface, the closure being realised by the assumption of local thermodynamic equilibrium at the interface.
A second important difference is made for the computation of the liquid heat transfer flux. In AS89 multi-D motion inside the droplet was considered through a reduction method to compute the interfacial heat flux. In the present work, the temperature inside the drop is assumed to obey a specific profile, corresponding to a boundary layer near the interface and a core zone at uniform temperature. The boundary layer thickness is determined from the assumed temperature profile and knowledge of the liquid average temperature. The average liquid temperature is a direct consequence of the two-phase average flow model resolution.
With this method, no parameter is present and two observations appear:
- The interfacial heat flux is in perfect agreement with the direct resolution of the heat equation inside the drop at any time.
- The only constraint used is energy conservation through the explicit use of the average liquid temperature.
Therefore, whatever the flow complexity is inside the drop, the present approach provides accurate interfacial heat flux provided that a core zone with uniform temperature is present and connected to the interface through a boundary layer profile. No internal mesh to the liquid droplet is used.
The mass transfer model thus consists in a set of three non-linear algebraic equations. There is no parameter in the model except physical properties of fluids in presence. The solution of this system is reached numerically in each computational cell and at each time step of the two-phase average equations resolution. It results in the computation of the mass flow rate from liquid to gas, positive in evaporation conditions and negative in condensation. It also provides mass, momentum and energy transfer terms to embed in volume average two-phase flow models.
The paper is organized as follows. The two-phase flow model under examination, with heat and mass transfers added as source terms is presented in Section 2. The conventional closure relations of this model are addressed in Section 3. The local and symmetric heat and mass transfer model for a single liquid droplet is built in Section 4. The local thermodynamic equilibrium interface condition is derived in Section 5. The heat exchange coefficients, in particular the one related to heat exchange internal to the droplet are determined in Section 6. The heat and mass transfer sub-model resolution method is given in Section 7 and validation results are shown in Section 8.

2. Two-phase flow model and properties

Two phases are considered here: gas (g) and liquid (L). The hydrodynamic part of the model is based on the Saurel and al. (2003) symmetric variant of the Baer and Nunziato (1986) model. Heat and mass transfers have been added as source terms.

Gas phase

$$\frac{\partial \alpha_g}{\partial t} + u_I \frac{\partial \alpha_g}{\partial x} = \mu\left(p_g - p_L\right) + \frac{A_I \dot{m}_g}{\rho_I}$$

$$\frac{\partial \alpha_g \rho_g Y_{g,air}}{\partial t} + \frac{\partial \alpha_g \rho_g Y_{g,air} u_g}{\partial x} = A_I \dot{m}_g \left(1 - Y_{g,wat,I}\right)$$

$$\frac{\partial \alpha_g \rho_g Y_{g,wat}}{\partial t} + \frac{\partial \alpha_g \rho_g Y_{g,wat} u_g}{\partial x} = A_I \dot{m}_g Y_{g,wat,I}$$

$$\frac{\partial \alpha_g \rho_g u_g}{\partial t} + \frac{\partial \alpha_g \rho_g u_g^{\,2} + \alpha_g p_g}{\partial x} = p_I \frac{\partial \alpha_g}{\partial x} + \lambda\left(u_L - u_g\right) + A_I \dot{m}_g u_I \qquad (1)$$

$$\frac{\partial \alpha_g \rho_g E_g}{\partial t} + \frac{\partial \alpha_g \left(\rho_g E_g + p_g\right) u_g}{\partial x} = P_I u_I \frac{\partial \alpha_g}{\partial x} + \lambda \overline{u_I}\left(u_L - u_g\right) - \mu \overline{p_I}\left(p_g - p_L\right)$$
$$- \frac{A_I \dot{m}_g p_I}{\rho_I} + A_I \dot{m}_g \left[Y_{g,wat,I} H_{g,wat,I} + \left(1 - Y_{g,wat,I}\right) H_{g,air,I} \right]$$
$$+ A_I H_{Tg}\left(T_I - T_g\right)$$

Liquid phase

$$\frac{\partial \alpha_L}{\partial t} + u_I \frac{\partial \alpha_L}{\partial x} = -\mu\left(p_g - p_L\right) - \frac{A_I \dot{m}_g}{\rho_I}$$
$$\frac{\partial \alpha_L \rho_L}{\partial t} + \frac{\partial \alpha_L \rho_L u_L}{\partial x} = -A_I \dot{m}_g \qquad (2)$$
$$\frac{\partial \alpha_L \rho_L u_L}{\partial t} + \frac{\partial \alpha_L \rho_L u_L^{\,2} + \alpha_L p_L}{\partial x} = p_I \frac{\partial \alpha_L}{\partial x} - \lambda\left(u_L - u_g\right) - A_I \dot{m}_g u_I$$
$$\frac{\partial \alpha_L \rho_L E_L}{\partial t} + \frac{\partial \alpha_L \left(\rho_L E_L + p_L\right) u_L}{\partial x} = p_I u_I \frac{\partial \alpha_L}{\partial x} - \lambda \overline{u_I}\left(u_L - u_g\right) + \mu \overline{p_I}\left(p_g - p_L\right)$$
$$+ \frac{A_I \dot{m}_g p_I}{\rho_I} - A_I \dot{m}_g H_{L,I} + A_I H_{TL}\left(T_I - T_c\right)$$
$$\frac{\partial \alpha_L \rho_L n_L}{\partial t} + \frac{\partial \alpha_L \rho_L u_L n_L}{\partial x} = \alpha_L \rho_L \dot{n}_L$$

This model considers each phase as compressible, evolving with its own velocity, temperature and pressure. The notations are conventional in the two-phase flow literature. The variable α_k represents the volume fraction of phase k ($k \in \{g,L\}$), such that $\sum_k \alpha_k = 1$. ρ, u, P, T, e and E represent respectively the density, the velocity, the pressure, the temperature, the internal energy and the total energy ($E = e + \frac{1}{2}u^2$).

The gas phase contains two chemical species, air and water vapour, whose mass concentrations are denoted by $Y_{g,air}$ and $Y_{g,wat}$ respectively. Obviously, $Y_{g,air} + Y_{g,wat} = 1$.

In the absence of source terms, it can be shown easily that this system is hyperbolic with wave speeds u_I, $u_k \pm c_k$ and u_k for $k \in \{g,L\}$.

Closure relations are needed for the practical use of these equations. Some of them are conventional while others, in particular those related to heat and mass transfer, are the aim of the present paper.

3. Conventional closure relations

Many closure relations and correlations are needed. For the sake of simplicity the most popular ones are presented hereafter.

3.1 Equations of state

The gas phase is assumed governed by the ideal gas equations of state:

$p_g = \rho_g R_g T_g$,

with $R_g = \frac{\hat{R}}{\hat{M}_g}$; $\hat{R} = 8.314 J.K^{-1}.mol^{-1}$ and ,

$\frac{1}{\hat{M}_g} = \frac{Y_{g,air}}{M_{g,air}} + \frac{Y_{g,wat}}{M_{g,wat}}$, with $\begin{cases} M_{g,air} = 29\times10^{-3} kg.mol^{-1} \\ M_{g,wat} = 18\times10^{-3} kg.mol^{-1} \end{cases}$.

The temperature is deduced from the caloric equation of state,

$$e_g - \sum_{j=air,wat} Y_{gj} e_j^0 = \int_0^T \sum_{j=air,wat} Y_{gj} c_{vj} dT,$$

with $e_{wat}^0 = 2030 kJ/kg$ and $e_{air}^0 = 0$.

The specific heats at constant volume $c_{v,j}$ are taken from the CHEMKIN-II thermodynamic database (Robert, 1989).

The liquid phase is assumed governed by the stiffened gas equation of state (Le Metayer et al., 2004):

$p_L = (\gamma_L - 1)\rho_L (e_L - e_L^0) - \gamma_L p_{\infty,L}$,

with $\gamma_L = 2.35$, $p_{\infty,L} = 10^9 Pa$ and $e_L^0 = -1167 kJ/kg$, this last parameter being linked to the liquid water specific heat of formation.

This EOS involves both molecular thermal agitation through the term $(\gamma_L - 1)\rho_L \left(e_L - e_L^0\right)$ and attractive short distance intermolecular effects through the term $-\gamma_L p_{\infty,L}$.

The associated caloric equation of state reads,

$$e_L = c_{v,L} T_L + \frac{p_{\infty,L}}{\rho_L} + e_L^0,$$

with $c_{v,L} = 1816 J.kg^{-1}.K^{-1}$

Obviously, both liquid and gas may be governed by other equations of state. Here, the liquid and gas parameters are such that the phase diagram is correctly reproduced in a given temperature range (Le Metayer et al., 2004).

3.2 Interfacial variables

The interfacial pressure and velocity are expressed with symmetric formulas with respect to the phase's indexes,

$$p_I = \frac{Z_L p_g + Z_g p_L}{Z_g + Z_L} + sgn\left(\frac{\partial \alpha_g}{\partial x}\right)\frac{Z_g Z_L}{Z_g + Z_L}\left(u_L - u_g\right),$$

$$u_I = \frac{Z_g u_g + Z_L u_L}{Z_g + Z_L} + sgn\left(\frac{\partial \alpha_g}{\partial x}\right)\frac{p_L - p_g}{Z_g + Z_L},$$

where $Z_k = \rho_k c_k$ represents the acoustic impedance of phase k with c_k the associated sound speed. These interfacial variables control the dynamics of droplet clouds, as they express velocity transport and forces acting at volume fraction gradients. They are consequences of local Riemann problem resolution in volume fraction gradient zones (Saurel et al., 2003).

The volume average pressure and interface velocities are given by,

$$\overline{u}_I = \frac{Z_g u_g + Z_L u_L}{Z_g + Z_L},$$

$$\overline{p}_I = \frac{Z_L p_g + Z_g p_L}{Z_g + Z_L}.$$

These variables express the transport velocity and pressure force acting inside the cloud of droplets.

The interfacial density appearing in the first equation of System (1) is expressed as well by a symmetric formula with respect to the phases (Saurel et al., 2008):

$$\rho_I = \frac{\frac{\rho_g c_g^2}{\alpha_g} + \frac{\rho_L c_L^2}{\alpha_L}}{\frac{c_g^2}{\alpha_g} + \frac{c_L^2}{\alpha_L}}.$$

When the gas phase is much compressible than the liquid phase, these formulas tend to,

$p_I \to p_g$; $\overline{p}_I \to p_g$; $u_I \to u_L$; $\overline{u}_I \to u_L$ and $\rho_I \to \rho_L$.

and the limit estimates of Baer and Nunziato (1986) are recovered. However, in specific thermodynamic conditions, such as in detonation waves for example, the gas compressibility is comparable to the one of the liquid and validity of these limit estimates fails.

The interfacial total enthalpies $H_{g,wat,I}$, $H_{g,air,I}$ and $H_{L,I}$ require the determination of the interfacial temperature T_I, whose determination will be addressed in Section 4. Stagnation interfacial enthalpies are defined as:

$$H_{g,wat,I} = c_{p,g,wat} T_I + e^0_{wat} + \frac{1}{2} u_I^2$$

$$H_{g,air,I} = c_{p,g,air} T_I + e^0_{air} + \frac{1}{2} u_I^2$$

$$H_{L,I} = c_{p,L} T_I + e^0_L + \frac{1}{2} u_I^2$$

with $c_{p,g,wat} = 1487\ \text{J.kg}^{-1}.\text{K}^{-1}$, $c_{p,g,air} = 1007\ \text{J.kg}^{-1}.\text{K}^{-1}$ and $c_{p,L} = \gamma_L c_{v,L}$.

3.3 Mechanical relaxation rates

The pressure relaxation is controlled by the following relaxation parameter:

$$\mu = \frac{A_I}{Z_g + Z_L}.$$

In practical computations, as the pressure relaxation time is typically less than one micro-second (Chinnayya et al., 2004), instantaneous pressure relaxation is achieved after each computational time step with the help of relaxation solvers such as those given in Lallemand and Saurel (2000). With stiff pressure relaxation solvers knowledge of the relaxation parameter μ and specific interfacial area A_I are useless. However, the interfacial area is needed to express drag effects as well as heat and mass transfers as they occur through interfaces on typical time scales much larger than the pressure relaxation one.

The specific interfacial area is expressed from the particle droplet size, that is evolving in the present context as mass transfer is considered. Here, the droplets are assumed spherical with the same average size (radius r_L) given by:

$$\alpha_L = \frac{4}{3}\pi r_L^3(\alpha_L \rho_L n_L) \text{ or alternatively, } r_L = \left(\frac{3}{4\pi\rho_L n_L}\right)^{1/3}. \quad (3)$$

The number density of particles per unit mass n_L is necessary to compute the particle radius. Its evolution is given by the last equation of System (2). The product $(\alpha_L \rho_L n_L)$ can also be denoted as N_L, the number density per unit volume.

When the particle radius is determined, there is no difficulty to compute the specific interfacial area,

$A_I = 4\pi r_L^2(\alpha_L \rho_L n_L)$.

In this equation, a **droplet fragmentation** term may be present $\dot{n}_L$. This source term is estimated with the algorithm that follows:

- The fragmentation time t_F is computed as,

$$t_F = \tau \frac{2r_L}{|u_L - u_g|}\sqrt{\frac{\rho_L}{\rho_g}},$$

where τ is a dimensionless time given by correlations based on the Weber number (Pilch and Erdman, 1987). It reads,

$$\tau = \frac{\pi}{4}\left[\frac{\sigma}{\rho_l D^3} - 6.25\frac{\mu_l}{\rho_l D^2}\right]^{-0.5} \qquad We \le 12$$

$$\tau = 6(We-12)^{-0.25} \qquad 12 < We \le 18$$

$$\tau = 2.45(We-12)^{0.25} \qquad 18 < We \le 50$$

$$\tau = 14.1(We-12)^{-0.25} \qquad 50 < We \le 350$$

$$\tau = 0.766(We-12)^{0.25} \qquad 350 < We \le 2760$$

$$\tau = 5.5 \qquad 2760 < We$$

The Weber number is defined as,

$$We = \frac{2\rho_g |u_L - u_g|^2 r_L}{\sigma},$$

where σ denotes the liquid-gas surface tension coefficient.

- The droplet radius at the end of the fragmentation process is estimated as,

$$r_f = \frac{\sigma We^*}{2\rho_g |u_L - u_g|^2},$$

where We* =12 denotes the critical Weber number, the lower limit of the fragmentation process.

From these relations the following relaxation equation is obtained for the droplet size determination:

$$\frac{dr_L}{dt} = \frac{r_f - r_L}{t_F}.$$

With the help of Relation (3) and mass conservation equation of System (2) it becomes:

$$\frac{\partial \alpha_L \rho_L n_L}{\partial t} + \frac{\partial \alpha_L \rho_L u_L n_L}{\partial x} = -\frac{3\alpha_L \rho_L}{r_L}\frac{r_f - r_L}{t_F}.$$

As the droplet radius decreases during fragmentation, the number density increases.

To close this mechanical relaxation subsection it remains to examine velocity relaxation.

Drag effects

The drag parameter λ appearing in systems (1) and (2) is actually a function of the particle Reynolds number defined as,

$$\mathrm{Re}_p = \frac{2\rho_g r_L \left\| \vec{u}_g - \vec{u}_l \right\|}{\mu_g},$$

where μ_g represents the gas viscosity.

With the help of this Reynolds number it is possible to determine the drag coefficient (Clift et al., 1978),

$$\mathrm{Cd} = \begin{cases} \dfrac{24}{\mathrm{Re}_p}(1 + 0.15\,\mathrm{Re}_p^{0.687}) & \text{if} \quad \mathrm{Re}_p < 1000 \\ 0.432 & \text{otherwise} \end{cases}.$$

Then, the drag parameter is obtained as,

$$\lambda = \frac{3\alpha_L C_d \alpha_g \rho_g \left| u_g - u_L \right|}{8 r_L}.$$

Conventional closure relations being now given, we now address the aim of the present paper,

i.e., heat and mass transfer closure relations.

4. Building the symmetric heat and mass transfer model

We now address building of the algebraic flow model to determine the last unknown functions appearing in Systems (1-2):

- The gas mass flow rate $\dot{m}_g$.
- The interfacial temperature T_I.
- The interfacial water vapor mass fraction in the gas phase $Y_{g,wat,I}$.

The gas heat exchange coefficient H_{Tg} is determined on the basis of conventional Nusselt number correlations while the internal heat exchange coefficient H_{TL} and the droplet core temperature T_c (appearing in the liquid energy equation of System 2) will be the subject of special attention in a forthcoming section.

The algebraic system giving the three unknowns $\dot{m}_g$, T_I and $Y_{g,wat,I}$ is a consequence of jump conditions of mass, energy and local thermodynamic equilibrium. These jump conditions derive of local balance equations of mass and energy in each phase.

4.1 Interface conditions

Local balance equations

In the present approach drops are made of pure liquid and surrounded by a pure gas mixture made of air and water vapour.

The mass conservation equation for each chemical species $i \in \{\mathrm{air}, \mathrm{wat}\}$ in a given phase $k \in \{L, g\}$ reads:

$$\frac{\partial \rho_k Y_{k,i}}{\partial t} + \vec{\nabla} \cdot \left(\rho_k Y_{k,i} \vec{u}_k - \rho_k D_{k,i} \vec{\nabla}(Y_{k,i}) \right) = 0 .$$

In the gas phase, it is assumed that each mass diffusion coefficients $D_{g,air} = D_{g,wat} = D_g$ are equal. In the liquid phase, knowledge of this coefficient is useless as the liquid is assumed pure: $Y_{L,air} = 0$ and $Y_{L,water} = 1$.
Neglecting viscous dissipation the energy conservation equation for each phase k reads,

$$\frac{\partial \rho_k E_k}{\partial t} + \vec{\nabla} \cdot \left(\rho_k E_k \vec{u}_k + p_k \vec{u}_k + \vec{q}_k \right) = 0 , \; k \in \{g, L\},$$

where $\vec{q}_k$ denotes the heat flux,

$$\vec{q}_k = -\lambda_{T,k} \vec{\nabla} T_k - \rho_k D_k \sum_i h_{k,i} \vec{\nabla} Y_{k,i} ,$$

and $\lambda_{T,k}$ denotes the phase k thermal conductivity.

In the following, the flow is assumed isobaric and at low Mach number in both phases, similarly as in flames dynamics. These assumptions are realistic as evaporation fronts propagate at low speed compared to the speed of sound. Acoustic waves propagate fast and are responsible for pressure uniformity, at least at leading order. Two consequences follow:

- The energy equation reduces to,

$$\frac{\partial \rho_k e_k}{\partial t} + \vec{\nabla} \cdot \left(\rho_k h_k \vec{u}_k + \vec{q}_k \right) = 0 ,$$

where e_k and h_k represent respectively the specific internal energy and enthalpy ($h_k = e_k + \frac{p_k}{\rho_k}$).

- The momentum equation is replaced by the uniform pressure condition.

The above mass and energy equations being frame invariant the system remains the same when expressed in the frame of the interface. The only change appears in the definition of the phases velocity,

$$\hat{u}_k = \vec{u}_k - \vec{\sigma} ,$$

where $\vec{\sigma}$ represents the local interfacial velocity.

With these notations the system reads,

$$\frac{\partial \rho_k Y_{k,i}}{\partial t} + \nabla . \left(\rho_k Y_{k,i} \hat{u}_k - \rho_k D_k \nabla Y_{k,i} \right) = 0 \qquad (4)$$

$$\frac{\partial \rho_k E_k}{\partial t} + \nabla \cdot \left(\rho_k h_k \hat{u}_k + \vec{q}_k \right) = 0 ,$$

with $\vec{q}_k = -\lambda_{T,k} \vec{\nabla} T_k - \rho_k D_k \sum_i h_{k,i} \vec{\nabla} Y_{k,i}$, $i \in \{air, wat\}$ and $k \in \{L, g\}$.

In the following, the notation '$\hat{}$' is omitted.

Jump conditions

The following picture represents a control volume at the drop boundary.

System (4) is integrated in the control volume schematized in Figure 1. The local interface velocity σ is assumed constant so that the flow configuration is steady and the time derivatives of the System (4) vanish. It means that the drop is large enough or that the front velocity is not varying significantly in the time range of observation. Thanks to these assumptions System (4) imply the following jump conditions:

$$\int_{S_g} \left(\rho_g Y_{g,i} \vec{u}_g - \rho_g D_g \vec{\nabla} Y_{g,i}\right).\vec{n}_g \, dS + \int_{S_L} \left(\rho_L Y_{L,i} \vec{u}_L - \rho_L D_L \vec{\nabla} Y_{L,i}\right).\vec{n}_L \, dS = 0 \tag{5}$$

$$\int_{S_g} \left(\rho_g h_g \vec{u}_g + \vec{q}_g\right).\vec{n}_g \, dS + \int_{S_L} \left(\rho_L h_L \vec{u}_L + \vec{q}_L\right).\vec{n}_L \, dS = 0 \tag{6}$$

where $\vec{n}_g$ and $\vec{n}_L$ denote the outward unit normal vectors of the corresponding phases. When the lateral surface ε tends to zero the liquid and gas surfaces S_g and S_L merge.

4.2 Examination of the mass interface condition

For each species $i \in \{air, wat\}$, equation (5) implies:

$$\left(\rho_g Y_{g,i} \vec{u}_g - \rho_g D_g \vec{\nabla} Y_{g,i}\right).\vec{n}_g + \left(\rho_L Y_{L,i} \vec{u}_L - \rho_L D_L \vec{\nabla} Y_{L,i}\right).\vec{n}_L = 0$$

Upon summation it reads,

$$\left(\rho_g \vec{u}_g \sum_i Y_{g,i} - \rho_g D_g \sum_i \vec{\nabla} Y_{g,i}\right).\vec{n}_g + \left(\rho_L \vec{u}_L \sum_i Y_{L,i} - \rho_L D_L \sum_i \vec{\nabla} Y_{L,i}\right).\vec{n}_L = 0$$

and simplifies as,

$$\sum_k \rho_k \vec{u}_k . \vec{n}_k = 0$$

i.e.,

$$\dot{m}_g + \dot{m}_L = 0 \ , \tag{7}$$

with the following definition for the mass flux: $\dot{m}_k = \rho_k \vec{u}_k . \vec{n}_k$.

The conservation equation for each chemical species i then reads :

$$\dot{m}_g Y_{g,i} - \rho_g D_g \vec{\nabla} Y_{g,i} . \vec{n}_g + \dot{m}_L Y_{L,i} - \rho_L D_L \vec{\nabla} Y_{L,i} . \vec{n}_L = 0$$

The liquid being pure extra simplification appears:

$$\dot{m}_g Y_{g,i} - \rho_g D_g \vec{\nabla} Y_{g,i} . \vec{n}_g + \dot{m}_L Y_{L,i} = 0 \tag{8}$$

Furthermore, considering Fick's first law of diffusion for each species of the gas phase,

$\vec{J}_{g,i} = -\rho_g D_g \vec{\nabla} Y_{g,i}$,

Equation (8) becomes,

$\dot{m}_g Y_{g,i} + \vec{J}_{g,i}.\vec{n}_g + \dot{m}_L Y_{L,i} = 0$

As $\sum_i Y_{g,i} = 1$ it implies $\vec{\nabla}\left(\sum_i Y_{g,i}\right) = 0$ and consequently $\sum_i \vec{J}_{g,i} = 0$.

It's worth to mention that the above simplified expressions are differential equations since gradients are present in the Fick's law. In order to transform these ODEs to an algebraic system mass exchange coefficient is introduced:

$\vec{J}_{g,i} = \rho_g H_{Mg}\left(Y_{g,i,I} - Y_{g,i,\infty}\right)\vec{n}_g$

where,

- $Y_{g,i,I}$ denotes the concentration of species i in the phase g at the interface,
- $Y_{g,i,\infty}$ represents the concentration of species i in the phase g far from the interface,
- H_{Mg} denotes the mass exchange coefficient in the gas phase.

Estimation of the mass exchange coefficient

The mass exchange coefficient between the gas phase and the interface is expressed with the help of the Sherwood number definition:

$S_h = \frac{2 r_L H_{Mg}}{D_g}$.

Sherwood number correlations are deduced from Nusselt number ones. The popular Frossling (1956) correlation is reported hereafter:

$N_u = 2 + 0.522 R_{ep}^{1/2} P_r^{1/3}$ (9)

The particle Reynolds number R_{ep} has already been defined and the Prandtl number P_r is defined as:

$P_r = \frac{\mu_v c_p}{\lambda_{T,g}}$,

with μ_v the gas dynamic viscosity, c_p the gas heat capacity at constant pressure and $\lambda_{T,g}$ the gas thermal conductivity.

The Sherwood number is deduced from (9),

$S_h = 2 + 0.522\, R_{ep}^{1/2} S_c^{1/3}$,

where S_c is the Schmidt number defined by,

$S_c = \frac{\mu_v}{\rho_g D_g}$.

Algebraic form of the mass interface condition

Thanks to the previous definitions it is possible to express System (8) as,

$$\dot{m}_g Y_{g,air,I} + \rho_g H_{Mg}\left(Y_{g,air,I} - Y_{g,air,\infty}\right) = 0$$

$$\dot{m}_g Y_{g,wat,I} + \rho_g H_{Mg}\left(Y_{g,wat,I} - Y_{g,wat,\infty}\right) + \dot{m}_L = 0$$

As their sum reduces to,

$$\dot{m}_g + \dot{m}_L = 0\,,$$

the gas mass flux reads,

$$\dot{m}_g = \frac{\rho_g H_{Mg}\left(Y_{g,wat,I} - Y_{g,wat,\infty}\right)}{1 - Y_{g,wat,I}} \qquad (10)$$

This equation expresses the gas mass flow rate emitted by a liquid surface under the sole effect of molecular mass diffusion. Such mass flux is valid when the liquid and gas temperatures are in equilibrium, as for example when a wet piece of cloth is put in dry air or inversely when a dry cloth is put in humid air.

Thereafter energetic effects are considered as they are of leading importance when thermal disequilibrium is present.

4.3 Examination of the energy jump relation at the interface

Equation (6) implies,

$$\left(\rho_g h_g \vec{u}_g + \vec{q}_g\right).\vec{n}_g + \left(\rho_L h_L \vec{u}_L + \vec{q}_L\right).\vec{n}_L = 0\,, \qquad (11)$$

where the heat flux is given by the sum of the Fourier's law and energy transport by mass diffusion terms,

$$\vec{q}_k = -\lambda_{t,k}\vec{\nabla}T_k - \rho_k D_k \sum_i h_{k,i}\vec{\nabla}Y_{k,i}\,,\quad i \in \{air, wat\} \text{ and } k \in \{L, g\}.$$

The enthalpy of the phase k is defined by $h_k = \sum_i Y_{k,i} h_{k,i}$.

In the liquid phase, the heat flux reduces to $\vec{q}_L = -\lambda_{T,L}\vec{\nabla}T_L$

With the help of the mass flux definition (11) becomes,

$$\dot{m}_g h_g + \vec{q}_g.\vec{n}_g + \dot{m}_L h_L + \vec{q}_L.\vec{n}_L = 0\,.$$

Inserting the heat flux definition it becomes,

$$\dot{m}_g \sum_i Y_{g,i} h_{g,i} - \rho_g D_g \sum_i h_{g,i}\vec{\nabla}Y_{g,i}.\vec{n}_g - \lambda_{T,g}\vec{\nabla}T_g.\vec{n}_g + \dot{m}_L \sum_i Y_{L,i} h_{L,i} - \lambda_{T,l}\vec{\nabla}T_L.\vec{n}_L = 0$$

or,

$$\sum_i h_{g,i}\left(\dot{m}_g Y_{g,i} - \rho_g D_g \vec{\nabla} Y_{g,i}.\vec{n}_g\right) - \lambda_{T,g}\vec{\nabla} T_g.\vec{n}_g + \sum_i h_{L,i}\dot{m}_L Y_{L,i} - \lambda_{T,L}\vec{\nabla} T_L.\vec{n}_L = 0$$

With the help of the mass conservation at the interface for each species i,

$\dot{m}_g Y_{g,i} - \rho_g D_g \vec{\nabla} Y_{g,i}.\vec{n}_g + \dot{m}_L Y_{L,i} = 0$,

the energy equation becomes,

$$\sum_i \left(h_{L,i} - h_{g,i}\right)\dot{m}_L Y_{L,i} - \lambda_{T,g}\vec{\nabla} T_g.\vec{n}_g - \lambda_{T,L}\vec{\nabla} T_L.\vec{n}_L = 0$$

As done previously with mass exchanges, the Fourier's law is re-expressed with the help of a heat exchange correlation,

$$-\lambda_{T,k}\vec{\nabla} T_k.\vec{n}_k = H_{Tk}\left(T_I - T_{k,\infty}\right) \qquad (12)$$

where,

- H_{Tk} represents the heat exchange coefficient, whose determination will be addressed later, particularly in the liquid phase.
- T_I represents the interfacial temperature.
- $T_{k,\infty}$ denotes the temperature of the phase k far from the interface. In particular $T_{L,\infty} = T_c$, the droplet core temperature.

The energy jump relation at the interface now becomes:

$$\sum_i \left(h_{l,i} - h_{g,i}\right)\dot{m}_l Y_{l,i} + H_{Tg}\left(T_I - T_{g,\infty}\right) + H_{TL}\left(T_I - T_c\right) = 0$$

In the liquid phase as $Y_{l,air} = 0$ and $Y_{l,water} = 1$ the previous equation then reads:

$$\left(h_{L,wat,I} - h_{g,wat,I}\right)\dot{m}_L + H_{Tg}\left(T_I - T_{g,\infty}\right) + H_{TL}\left(T_I - T_c\right) = 0\,.$$

Using the interface mass condition (7), a second expression for the gas mass flux appears:

$$\dot{m}_g = \frac{H_{Tg}\left(T_{g,\infty} - T_I\right) + H_{TL}\left(T_c - T_I\right)}{L_{v,wat}\left(T_I\right)}\,, \qquad (13)$$

where $L_{v,wat}\left(T_I\right) = h_{g,wat,I} - h_{L,wat,I}$ represents the latent heat of vaporization.

Relation (13) can be used to determine the mass flow rate when molecular mass diffusion is absent. Such situation corresponds for example to the case of a liquid drop placed in its vapour.

In this case, the interface mass condition (10) is not defined and not considered for the mass transfer rate determination.

When both molecular and heat diffusion effects are present both relations (10) and (13) must be considered. This system involves the following unknowns,

$\dot{m}_g$, $Y_{g,wat,I}$, T_I, H_{TL} and T_c.

As only two relations are available at present (Relations 10 and 13), closure relations are needed.

The heat transfer coefficient internal to the liquid phase and the droplet core temperature determination will be addressed in Section 6. We now address mass concentration $Y_{g,wat,I}$ determination at the interface.

5. Local thermodynamic equilibrium

The interface is assumed at local thermodynamic equilibrium, meaning:

- $T_{g,I} = T_{L,I} = T_I$ (local thermal equilibrium),
- $p_{g,I} = p_{L,I} = p_I = p$ (mechanical equilibrium), (14)
- $g_{g,I} = g_{l,I}$ (chemical equilibrium – see Appendix A for details regarding this relation).

g_k represents the Gibbs free energy of a given phase ($g_k = h_k - T_k s_k$).
In the second relation of System (14) surface tension effects have been neglected.
Any thermodynamic state function, such as g_k is function of two thermodynamic variables: $g_k = g_k(T_k, p_k)$. From System (14) it appears that,
$g_{g,I}(T_I, p) = g_{L,I}(T_I, p)$.
This relation implies the well known saturation condition,
$T_I = T_{sat}(p)$ or alternatively, $p = p_{sat}(T_I)$.

In the present particular situation, the vapor partial pressure at the drop interface is equal to the saturation pressure at local temperature T_I :

$$p_{g,wat,I} = p_{sat,wat}(T_I) \tag{15}$$

The gas mixture is now assumed ideal in the sense that each gas is supposed to obey the ideal gas law. From the Dalton law for ideal gases, the gas mixture pressure is equal to the sum of the individual gas species partial pressures. In the present context the water vapor partial pressure obeys,

$$p_{g,wat,I} V_g = n_{g,wat,I} \hat{R} T_I ,$$

and the gas mixture obeys,

$$p V_g = \sum_i n_{g,i,I} \hat{R} T_I ,$$

both expressed in the gas at the interface.

Molar fractions are defined as,

$$x_{g,i} = \frac{n_{g,i}}{\sum_i n_{g,i}} .$$

Consequently,

$$x_{g,wat,I} = \frac{p_{g,wat,I}}{p} = \frac{p_{sat,wat}(T_I)}{p} .$$

It remains to convert mole to mass fractions:

$$Y_{g,i} = x_{g,i} \frac{M_{g,i}}{\hat{M}_g}$$

The water vapor mass fraction at the interface is thus given by,

$$Y_{g,wat,I} = \frac{\hat{M}_{g,wat}}{\hat{M}_g\left(Y_{g,wat,I}\right)} \frac{p_{sat,wat}\left(T_I\right)}{p} \tag{16}$$

with $\frac{1}{\hat{M}_g} = \frac{Y_{g,wat,I}}{\hat{M}_{wat}} + \frac{1-Y_{g,wat,I}}{\hat{M}_{air}}$.

Water saturation pressure

Based on the Rankine's popular relation for the saturation pressure as a function of temperature, we propose the following formula, valid in the temperature range $[273K, 647K]$:

$$p_{sat,wat}(T) = \exp\left(12.98 - \frac{4900}{T}\right) \text{bars}.$$

This relation represents very well the experimental curve, as shown in the Figure 2. It is also a very good approximation of the theoretical relation resulting of System (14) and stiffened gas equation of state for the liquid and vapor couple (Le Metayer et al., 2014).

System (10, 13, 16) corresponds now to an algebraic non-linear system with five unknowns, needing drops internal heat exchange H_{TL} and core temperature T_c determination. Their estimation is addressed in the next section.

6. Heat exchanges

The gas-interface heat exchange coefficient H_{Tg} is readily obtained from the Nusselt number correlation (9) and the following definition:

$$H_{Tg} = \frac{\lambda_{Tg} N_u}{2 r_L}.$$

Determination of the heat exchange coefficient internal to the droplet (H_{TL}), between its core and the interface is more challenging. Attempt in this direction was done in AS89 with a constant Nusselt number of 6.58, corrected by a coefficient to account for internal fluid motion.

The present contribution departs significantly from these authors at this level as we consider that unsteady effects in drop heating (or cooling in flashing situations) may be of primary importance. Indeed, whatever the multidimensional behavior the flow has in the droplet, at short time scales, a sharp thermal boundary layer develops at the interface. The boundary layer width is precisely linked to the interfacial heat flux, that may be very large at short time scales.

As we consider impossible to account precisely of recirculation effects inside the drop, at least with a fast method (0D or 1D), we examine an approach that:

- considers unsteadiness through radial 1D variable depth boundary layer,

- is free of adjustable parameter.

To do this the droplet is divided in two zones as shown in Figure 3.

This representation addresses short terms heating or cooling of drops. When the boundary layer reaches the drop center another representation is used, preserving continuity with the two temperature profiles.

The boundary layer thickness is determined unambiguously with the method that follows. It uses:
- Approximate temperature profiles, more based on physical arguments than any given set of partial differential equations, as we consider that their solution is unreachable.

- Knowledge of volume average liquid temperature, given by the energy equation of System (2).

This last information forces the subscale model and the average one to be compatible. In particular the subscale model doesn't address any set of PDEs but fulfills the only unambiguous data that are:

- Given surface temperature T_I as it is already an unknown of System (10, 13, 16).

- Liquid energy conservation.

6.1 Short-term solutions

Let's consider the following temperature profile:

$$\begin{cases} T = T_c + (T_I - T_c)\left(\dfrac{\delta - r}{\delta - r_L}\right)^n & \text{if} \quad 0 \le \delta \le r \le r_L \\ T = T_c & \text{otherwise} \end{cases} \tag{17}$$

where $r_L - \delta$ denotes the thermal boundary layer thickness. The parameter n is given. It will be shown latter that method's accuracy has weak dependence to this parameter.

The core temperature T_c is given too, as it corresponds in most situations to the initial liquid temperature or liquid temperature at injection. Thus, in most situations,

$T_c = \text{cst.}$

However, if the liquid is injected with time varying temperature, it will be necessary to add a transport equation to System (2):

$$\frac{\partial T_c}{\partial t} + \bar{u}_L.\text{grad}(T_c) = 0\,.$$

Now, if liquid compressibility induces large temperature variations, the core temperature will be better determined from the liquid entropy equation, to add to System (2) instead of the previous one,

$$\frac{\partial \alpha_L \rho_L s_L}{\partial t} + \frac{\partial \alpha_L \rho_L u_L s_L}{\partial x} = 0,$$

with a specific treatment at shocks, such as the one detailed in Petitpas et al. (2009).

From the temperature profile (17), when T_c is determined by one of the former methods the next step consists in the consideration of the local heat flux at the liquid interface:

$$\vec{q}_{L,I}.\vec{n}_L = -\lambda_{T,L} \left.\frac{\partial T}{\partial r}\right|_{r=r_L} \vec{u}_r.\vec{n}_L = \lambda_{T,L} \left.\frac{\partial T}{\partial r}\right|_{r=r_L} \equiv H_{TL}\left(T_I - T_c\right)$$

Using (17) in the previous relation implies:

$$\frac{\lambda_{T,L} n \left(T_I - T_c\right)}{\left(r_L - \delta\right)} = H_{TL}\left(T_I - T_c\right).$$

Thus,

$$H_{TL} = \frac{\lambda_{T,L} n}{\left(r_L - \delta\right)}. \tag{18}$$

The only remaining unknown is the distance δ. To determine it let's consider the volume average liquid drop temperature definition:

$$\overline{T}_L = \frac{1}{V}\int_0^{r_L} T dV = \frac{1}{\frac{4}{3}\pi {r_L}^3}\int_0^{r_L} T 4\pi r^2 dr = \frac{3}{{r_L}^3}\int_0^{r_L} T r^2 dr \tag{19}$$

Inserting the temperature profile (17) in (19) results in:

$$\overline{T}_L = \frac{3(r_L - \delta)}{{r_L}^3}\left[T_c\left(\delta^2 + \frac{(\delta - r_L)^2}{3} - \delta(\delta - r_L) - \frac{\delta^3}{3(\delta - r_L)} \right) + (T_I - T_c)\left(\frac{\delta^2}{n+1} - \frac{2\delta(\delta - r_L)}{n+2} + \frac{(\delta - r_L)^2}{n+3} \right) \right] \tag{20}$$

As $\overline{T}_L$ is an output of System (2), the only unknowns are δ and T_I. For a given T_I during the numerical resolution process of System (10, 13, 16), the distance δ is determined by solving (20) with the Newton-Raphson method.

6.2 Long-term solutions

"Long-term" profile happens when the boundary layer reaches the liquid drop center, e.g. $\delta = 0$. Setting $\delta = 0$ in (17) the "long -term" temperature profile is obtained:

$$T = T_c + \left(T_I - T_c\right)\left(\frac{r}{r_L}\right)^n \quad \text{if} \quad 0 \le r \le r_L \tag{21}$$

It is clear that this solution is continuity preserving with the former approximate solution (17).

Now the unknown is the liquid core temperature. But its determination isn't needed for the heat exchange coefficient H_{TL} calculation. Indeed,

$$\vec{q}_{L,I}.\vec{n}_L = -\lambda_{T,L}\left.\frac{\partial T}{\partial r}\right|_{r=r_L} \quad \vec{u}_r.\vec{n}_L = \lambda_{T,L}\left.\frac{\partial T}{\partial r}\right|_{r=r_L} \equiv H_{TL}\left(T_I - T_c\right)$$

Using (21) it appears,

$$\frac{\lambda_{T,L} n\left(T_I - T_c\right)}{r_L} = H_{TL}\left(T_I - T_c\right).$$

Thus,

$$H_{Tl} = \frac{\lambda_{t,l} n}{r_L} \tag{22}$$

In order to determine the core temperature T_c that appears in the heat exchange, we use the volume average liquid temperature definition (19). Inserting the temperature profile (21),

$$\overline{T_L} = \frac{3}{r_L{}^3}\int_0^{r_L}\left(T_c + \left(T_I - T_c\right)\left(\frac{r}{r_L}\right)^n\right) r^2 dr = T_c + 3\frac{\left(T_I - T_c\right)}{\left(n+3\right)},$$

resulting in an explicit formulation for T_c,

$$T_c = \frac{\left(n+3\right)\overline{T_L} - 3T_I}{n} \tag{23}$$

The "long-term" temperature profile is now determined for given n, T_I and $\overline{T}_L$.

6.3 Validation

System (2) is considered in the absence of fluid motion and without gradients of the various flow variables. Heat exchanges only are considered resulting in the following ODE system:

$$\begin{aligned}
&\frac{\partial \alpha_L}{\partial t} = -\mu\left(p_g - p_L\right)\\
&\frac{\partial \alpha_L \rho_L}{\partial t} = 0\\
&\frac{\partial \alpha_L \rho_L u_L}{\partial t} = 0\\
&\frac{\partial \alpha_L \rho_L E_L}{\partial t} = A_I H_{TL}\left(T_I - T_c\right) + \mu \overline{p}_I\left(p_g - p_L\right)
\end{aligned} \tag{24}$$

Assuming now weak pressure differential $\left(p_g - p_L\right)$ and weak liquid compressibility the energy equation becomes,

$$\frac{\partial \overline{T}_L}{\partial t} = \frac{3}{r_L \rho_L c_{vL}} H_{TL}\left(T_I - T_c\right) \tag{25}$$

Equation (25) is solved numerically with constant interface temperature T_I to provide the volume average temperature as a function of time $\overline{T}_L(t)$.

At each time step, the heat exchange coefficient is varying as a function of the core zone radius,

$$H_{TL}(\delta) = \begin{cases} \dfrac{\lambda_{T,L} n}{r_L - \delta} \text{ if } \delta \in]0; r_L[\\ \dfrac{\lambda_{t,l} n}{r_L} \text{ otherwise} \end{cases}.$$

Likewise, T_c varies as discussed in section 6.2.

Algorithm

The following algorithm is used to determine the liquid-interface heat exchange coefficient H_{TL} and associated time varying heat flux (for given exponent n and interfacial temperature T_I in the approximate temperature profile).

1. The mean liquid temperature $\overline{T}_L(t)$ is computed from (25) in 0D computations and from System (2) in 1D computations. At the initial state $\overline{T}^0 = T_c^0$ and $\delta^0 = R - \varepsilon$. Thus, $H_{TL}^0 = \dfrac{\lambda_{t,L} n}{\varepsilon}$.
2. We first consider the "short-term" stage. The core zone radius δ is determined by solving (20). If $\delta \in]0; r_L[$, then the "short-term" assumption is checked. The heat exchange coefficient is computed and the algorithm then goes to step 1 for the next time step.
3. If $\delta \leq 0$, the heat exchange coefficient H_{TL} has to be computed with the "long-term" solution. Therefore, the liquid core temperature T_c is computed with (23). The algorithm then goes to step 1 for the next time step.

Comparison with the heat equation

Let's consider the following data:

- Interfacial temperature : $T_I = 600K$
- Liquid drop core initial temperature : $T_c^0 = 300K$
- Liquid drop radius : $r_L = 100\mu m$
- Liquid thermal conductivity : $\lambda_{T,L} = 0.6788 W.m^{-1}.K^{-1}$
- Liquid drop density : $\rho_L = 1000 kg.m^{-3}$
- Liquid drop specific heat: $c_{p,L} = 4267.6 J.kg^{-1}.K^{-1}$

The first step with this method deals with the exponent n determination. To do this, let's compare the temperature profiles for "short-terms" and different values of n (Figure 4). It appears that the solution dependence to this parameter is of minor importance. Moreover the main goal of this method is to provide an accurate approximation of the interface heat flux. This doesn't require necessarily an accurate internal temperature profile.

To check time accuracy of the interface heat flux computation with the reduced method comparison is done with the heat equation:

$$\frac{\partial T}{\partial t} = \frac{D_{T,L}}{r^2} \frac{\partial}{\partial r}\left(r^2 \frac{\partial T}{\partial r} \right),$$

where $D_{T,L} = \dfrac{\lambda_{T,L}}{\rho_L c_{p,L}}$ represents the thermal diffusion coefficient in the drop.

Introducing the following change of variables,

$$\theta = \frac{T - T_c^0}{T_I - T_c^0},\ \eta = \frac{r}{r_L} \text{ and } \tau = \frac{D_L t}{{r_L}^2},$$

with T_c^0 the initial drop core temperature, the dimensionless heat equation reads:

$$\frac{\partial \theta}{\partial \tau} = \frac{1}{\eta^2}\frac{\partial}{\partial \eta}\left(\eta^2 \frac{\partial \theta}{\partial \eta}\right).$$

Consequently the interfacial heat flux reads,

$$\vec{q}_{L,I}.\vec{n}_L = \lambda_{T,L}\left.\frac{\partial T}{\partial r}\right|_{r=r_L} = \frac{\lambda_{T,L}\left(T_I - T_c^0\right)}{r_L}\left.\frac{\partial \theta}{\partial \eta}\right|_{\eta=1},$$

i.e.,

$$\frac{\vec{q}_{L,I}.\vec{n}_L}{\dfrac{\lambda_{T,L}\left(T_I - T_c^0\right)}{r_L}} = \left.\frac{\partial \theta}{\partial \eta}\right|_{\eta=1}.$$

The dimensionless heat flux $q_{HeatEq} = \left.\dfrac{\partial \theta}{\partial \eta}\right|_{\eta=1}$ is determined by solving the dimensionless heat equation with the help of finite differences. Then it is compared to the one determined with the approximate method,

$$q_{Method} = \frac{H_{TL}\left(T_I - T_c\right)}{\left(\dfrac{\lambda_{T,L}\left(T_I - T_c^0\right)}{r_L}\right)} = \frac{H_{TL} r_L \left(T_I - T_c\right)}{\lambda_{T,L}\left(T_I - T_c^0\right)}.$$

Corresponding results are shown in Figure 5 for two values of n. They show that the reduced method is accurate for the determination of the interface heat flux for both values of n.

These results show that the method is accurate for the interface heat flux computation at any time. In the rest of the paper, computations are made with $n = 2$.

7. Solving the local heat and mass transfer model

Having now in hands all closure relations to solve the mass transfer model we address its numerical resolution. This algebraic system is made of relations (10), (13) and (16):

$$\dot{m}_g = \frac{\rho_g H_{Mg}\left(Y_{g,wat,I} - Y_{g,wat,\infty}\right)}{1 - Y_{g,wat,I}} \qquad (26\text{-a})$$

$$\dot{m}_g = \frac{H_{Tg}\left(T_{g,\infty} - T_I\right) + H_{TL}\left(T_c - T_I\right)}{L_{v,wat}\left(T_I\right)} \tag{26-b}$$

$$Y_{g,wat,I} = \frac{M_{g,wat}}{\hat{M}_g\left(Y_{g,wat,I}\right)} \frac{p_{sat,wat}\left(T_I\right)}{p} \tag{26-c}$$

The system involves three unknowns: $\dot{m}_g$, $Y_{g,wat,I}$ and T_I. The core temperature T_c is assumed constant or determined by one of the equations of Sections 6.1 - 6.2.

Moreover, $T_{g,\infty}$ is assumed equal to the volume average gas temperature T_g.

However, this system is highly nonlinear and requires a specific resolution method.

Combining (26-a) and (26-b) by eliminating the mass flux the following identity is obtained,

$$\frac{\rho_g H_{Mg}\left(Y_{g,wat,I} - Y_{g,wat,\infty}\right)}{1 - Y_{g,wat,I}} = \frac{H_{Tg}\left(T_{g,\infty} - T_I\right) + H_{TL}\left(T_c - T_I\right)}{L_{v,wat}\left(T_I\right)}.$$

Rearranging it a function expressing the interfacial temperature as a function of the vapor mass fraction at the interface is obtained:

$$T_I\left(Y_{g,wat,I}\right) = \frac{H_{Tg}T_{g,\infty} + H_{Tl}T_c}{H_{Tg} + H_{Tl}} - \frac{L_{v,wat}\left(T_I\right)\rho_g H_{Mg}\left(Y_{g,wat,I} - Y_{g,wat,\infty}\right)}{\left(H_{Tg} + H_{Tl}\right)\left(1 - Y_{g,wat,I}\right)} \tag{27}$$

Equation (26-c) can be expressed as,

$$p_{sat,wat}\left(T_I\right) = \frac{\hat{M}_g\left(Y_{g,wat,I}\right)}{M_{g,wat}} p Y_{g,wat,I}.$$

Combining these two last relations the following function is obtained:

$$f\left(Y_{g,wat,I}\right) = p_{sat,wat}\left(\frac{H_{Tg}T_{g,\infty} + H_{TL}T_c}{H_{Tg} + H_{TL}} - \frac{L_{v,wat}\left(T_I\right)\rho_g H_{Mg}\left(Y_{g,wat,I} - Y_{g,wat,\infty}\right)}{\left(H_{Tg} + H_{TL}\right)\left(1 - Y_{g,wat,I}\right)}\right) - \frac{\hat{M}_g\left(Y_{g,wat,I}\right)}{M_{g,wat}} p Y_{g,wat,I} \tag{28}$$

Reversing Relation (27) $Y_{g,wat,I}$ can be expressed as a function of temperature T_I:

$$Y_{g,wat,I}\left(T_I\right) = \frac{Y_{g,wat,\infty} + \left(\dfrac{\dfrac{H_{Tg}T_{g,\infty} + H_{Tl}T_c}{H_{Tg} + H_{Tl}} - T_I}{\dfrac{\rho_g H_{Mg} L_{v,wat}}{H_{Tg} + H_{Tl}}}\right)}{1 + \left(\dfrac{\dfrac{H_{Tg}T_{g,\infty} + H_{Tl}T_c}{H_{Tg} + H_{Tl}} - T_I}{\dfrac{\rho_g H_{Mg} L_{v,wat}}{H_{Tg} + H_{Tl}}}\right)} \tag{29}$$

This expression will be convenient and of particular importance numerical resolution. Therefore, admissible temperature bounds have to be determined.

Mathematical analysis of function (29)

This function can be rewritten as follows:

$$Y_{g,wat,I}(T)=\frac{C+DY_{g,wat,\infty}-T}{C+D-T},\ \forall T\in\mathbb{R}_+^*-\{T_{ND}\}$$

with $T_{ND}=C+D$ and with the positive constants $C=\frac{H_{Tg}T_{g,\infty}+H_{Tl}T_c}{H_{Tg}+H_{Tl}}$ and $D=\frac{\rho_g H_{Mg}L_{v,wat}}{H_{Tg}+H_{Tl}}$.

The function is monoticaly decreasing in the interval $T\in\left]0,T_{ND}\right[\cup\left]T_{ND},+\infty\right[$,

$$\frac{dY_{g,wat,I}(T)}{dT}=-\frac{D\left(1-Y_{g,wat,\infty}\right)}{(C+D-T)^2}<0.$$

Moreover,

$$\lim_{T\to T_{ND}^-} Y_{g,wat,I}(T)=-\infty\ ;\quad \lim_{T\to T_{ND}^+} Y_{g,wat,I}(T)=+\infty\ ;\text{ and }\quad \lim_{T\to+\infty} Y_{g,wat,I}(T)=1.$$

By definition, the water vapor mass fraction at the interface has to respect the physical condition $0<Y_{g,wat,I}(T)<1$. This condition is only checked for $T\in\left]0;T_0\right[$, with $T_0=C+DY_{g,wat,\infty}<T_{ND}$.

Another physical bound has to be considered, i.e., the critical temperature of the liquid ($T_{crit}=647.14K$). The considered domain upper bound is consequently $\mathrm{Min}(T_0,T_{crit})$. The solution algorithm for System (26) is the one that follows.

Algorithm

1. Define the accuracy ε and chose an initial guess for $T_I=T_{I,new}=\frac{T_c+T_{g,\infty}}{2}$.
2. Determine the latent heat of vaporization $L_{v,wat}(T_{I,new})$.
3. Compute the liquid-interface heat exchange coefficient $H_{Tl}(T_{I,new})$.
4. Define admissible temperature bounds:
   $T_{min}=0.1\,K$
   $T_{max}=\mathrm{Min}(T_0-0.1,T_{crit}-0.1)$
5. Compute mass fraction bounds using relation (29):
   $Y_a=Y_{g,wat,I}(T_{max})$
   $Y_b=Y_{g,wat,I}(T_{min})$
6. The Ridders' method is used to solve $f(Y_{g,wat,I})=0$ on the domain $[Y_a,Y_b]$ resulting in $Y_{g,wat,I}$ determination.
7. Update the temperatures using relation (27):
   $T_{I,init}=T_{I,new}$
   $T_{I,new}=T_I(Y_{g,wat,I})$
8. If $|T_{I,new}-T_{I,init}|\geq\varepsilon$, go to step 2.
   Otherwise, $T_I=T_{I,new}$.

Then the gas mass flow rate $\dot{m}_g$ is determined with (26-a) or (26-b).

System (26) is now solved and its solution is inserted in Systems (1) and (2).

8. Computational examples and validations

A simple evaporation test is addressed first, in order to check flow variables relaxation towards their equilibrium value. Local heat and mass transfer model capabilities to deal with unsteady wave propagation (shock and expansion waves) are addressed secondly.

8.1. Relaxation towards equilibrium

In this test, gas and liquid phase volume fractions are respectively set initially to $\alpha_g = 0.999$ and $\alpha_L = 0.001$. The pressure is atmospheric ($10^5 \mathrm{Pa}$) and the initial water vapor mass fraction in the gas phase is set to 0.01. The initial gas phase temperature is $1000\mathrm{K}$ and the liquid phase is at $300\mathrm{K}$ initially. Moreover, the liquid droplet radius is set to $5\mu\mathrm{m}$. All variables are plotted versus time in Figure 7.

As liquid droplet evaporation occurs, the gas mass flow rate $\dot{m}_g$ is positive. Each variable gradually reaches its equilibrium. Let's note that the interfacial and average liquid temperatures are very close at any time and are reached by the gas temperature at the end of the evaporation process.

8.2. Shock tube with droplets

In all tests that follow, the hyperbolic part of the two-phase flow model (1-2) is solved with the method given in Furfaro and Saurel (2014).

A one-meter long shock tube contains gas and liquid phases with uniform volume fraction everywhere. The gas phase occupies most of the volume ($\alpha_g = 0.999$). The left chamber has the same high pressure for both phases ($10^6 \mathrm{Pa}$) while the right one has the same low pressure ($10^5 \mathrm{Pa}$) for both phases. Gas and liquid temperatures are both set to $300\mathrm{K}$ everywhere.

Therefore, in all tests that follow the core temperature T_c is a constant for short terms solutions as defined in Section 6.1 while for long terms, it is computed by (25).

In these computations the right-facing shock and left-facing expansion waves propagate in liquid-gas mixtures at thermodynamic equilibrium. For given initial temperature T^0 and pressure p^0, the initial water vapor mass fraction in the gas phase $Y^0_{g,wat}$ is determined from relation (26-c):

$$Y^0_{g,wat} = \frac{M_{g,wat}}{\hat{M}_g\left(Y^0_{g,wat}\right)} \frac{p_{sat,wat}\left(T^0\right)}{p^0}$$

where $$\frac{1}{\hat{M}_g\left(Y^0_{g,wat}\right)} = \frac{1 - Y^0_{g,wat}}{M_{g,air}} + \frac{Y^0_{g,wat}}{M_{g,wat}}$$

After straightforward manipulations it becomes,

$$Y^0_{g,wat} = \frac{\dfrac{M_{g,wat} p_{sat,wat}\left(T^0\right)}{M_{g,air} p^0}}{1 - \dfrac{p_{sat,wat}\left(T^0\right)}{p^0}\left(1 - \dfrac{M_{g,wat}}{M_{g,air}}\right)}.$$

Three successive tests are considered with different initial liquid droplet radii. In the first test (Figure 8), the droplet radius is set to $1\mu\mathrm{m}$. The second and third ones consider same initial

conditions and vary only droplet radius that is $10\mu m$ in results shown in Figure 9 and $100\mu m$ in Figure 10. Stiff pressure relaxation is used everywhere whereas velocity relaxation occurs with finite rate λ as given in Section 3.3. No droplet breakup effect is considered.
These tests are done with a uniform mesh involving 500 cells. The initial pressure discontinuity is located at x=0.5 m.

Let's first remark that relaxation effects imply shock waves dispersion, that do not appear as discontinuities on the various graphs. Second, as expected droplet size is of major importance on temperatures and velocities relaxation and evaporation/condensation mechanism.
When the initial droplet radius is very small ($1\mu m$) and for the considered initial liquid volume fraction ($\alpha_L = 0.001$), the interfacial area is big. Drag effects are thus stiff involving velocities merging and temperatures being close each other. Moreover, condensation appears through the rarefaction wave ($\dot{m}_g < 0$), increasing the droplet size. The same phenomenon is present through the shock wave, whereas evaporation prevails through the contact discontinuity ($\dot{m}_g > 0$).
When the droplet radius increases ($10\mu m$,$100\mu m$) for the same initial liquid volume fraction, relaxation effects are weaker as the interfacial area is smaller. As before, condensation through the shockwave and evaporation through the contact discontinuity are observable.
However, the droplet radius behavior is very different through the rarefaction wave, where evaporation now prevails. This is a consequence temperature disequilibrium and pressure drop effects.
It thus appears that changing only the droplet size, non intuitive effects appear, and condensation zones in the flow may become evaporating zones.

9. Conclusions

A variant of the AS89 model has been built. The new model considers both liquid and gas compressibility. It is symmetric in the sense that phase change may occur as a consequence of gas heating effects to the liquid phase and inversely to energy already stored in the droplets. Therefore the present model is valid in any kind of evaporating/condensing situation of gas liquid droplets two-phase flows.

Acknowledgement

This work has been presented at the Conservation Laws workshop hold in November 2014 at Stuttgart (Germany) to honour Professor Claus Dieter Munz the year of his 60th birthday. The authors are grateful to the organizers for their kind invitation.
Part of this work has been carried out in the framework of the Labex MEC (ANR-10-LABX-0092) and of the A*MIDEX project (ANR-11-IDEX-0001-02), funded by the « Investissements d'Avenir » French Government program managed by the French National Research Agency (ANR).

References

Abramzon, B. and Sazhin, S. (2005). Droplet vaporization model in the presence of thermal radiation. International Journal of Heat and Mass Transfer, 48(9), 1868-1873.

Abramzon, B., and Sirignano, W. A. (1989). Droplet vaporization model for spray combustion calculations. International journal of heat and mass transfer, 32(9), 1605-1618

Baer, M. R., and Nunziato, J. W. (1986). A two-phase mixture theory for the deflagration-to-

detonation transition (DDT) in reactive granular materials. Int. J. Multiphase Flow 12(6), 861-889
Chinnayya, A., Daniel, E. and Saurel, R. (2004). Modelling detonation waves in heterogeneous energetic materials. Journal of Computational Physics, 196(2), 490-538
Clift, R., Grace, J.R. and Weber, M.E. (1978) Bubbles, drops, and particles. Academic Press
Furfaro, D. and Saurel, R. (2014) A simple HLLC-type Riemann solver for compressible non-equilibrium two-phase flows. Computers and Fluids, submitted
Frossling, N. (1956) Evaporation, heat transfer, and velocity distribution in two-dimensional and rotationally symmetrical laminar boundary-layer flow. NASA Langley Report, USA
Lallemand, M. H. and Saurel, R. (2000). Pressure relaxation procedures for multiphase compressible flows. INRIA Report 4038
Law, C. K. (1982). Recent advances in droplet vaporization and combustion. Progress in energy and combustion science, 8(3), 171-201
Le Metayer, O., Massoni, J., & Saurel, R. (2004). Elaborating equations of state of a liquid and its vapor for two-phase flow models; Elaboration des lois d'etat d'un liquide et de sa vapeur pour les modeles d'ecoulements diphasiques.International Journal of Thermal Sciences, 43(3), 265-276
Petitpas, F., Saurel, R., Franquet, E., & Chinnayya, A. (2009). Modelling detonation waves in condensed energetic materials: Multiphase CJ conditions and multidimensional computations. Shock waves, 19(5), 377-401
Pilch, M. and Erdman, C.A. (1987) Use of breakup time data and velocity history data to predict the maximum size of stable fragments for acceleration-induced breakup of a liquid drop. Int. J. Multiphase Flow, 13(6), 741-757.
Robert, J. (1989). Chemkin-II: A Fortran chemical kinetics package for the analysis of gas-phase chemical kinetics. Sandia National Laboratories Report, SAND89-8009B
Saurel, R., Petitpas, F., & Abgrall, R. (2008). Modelling phase transition in metastable liquids: application to cavitating and flashing flows. Journal of Fluid Mechanics, 607, 313-350.
Saurel, R., Le Martelot, S., Tosello, R. and Lapebie, E. (2014) Symmetric model of compressible granular mixtures with permeable interfaces. Phys. Fluids, in press
Sirignano, W. A. (2014). Advances in droplet array combustion theory and modeling. Progress in Energy and Combustion Science, 42, 54-86
Spalding, D. B. (1953). The combustion of liquid fuels. In Symposium (Int.) on combustion 4(1), 847-864
Stokes, G.G. (1851) On the effect of the internal friction of fluids on the motion of pendulums. Transactions of the Cambridge Philosophical Society, Volume 9.
Williams, F. A. (1958). Spray combustion and atomization. Physics of Fluids 1(6), 541-545

Appendix A – Phase equilibrium

Each chemical reaction or phase transformation involves reactants and products. In phase equilibrium the concentrations on both sides of the reaction are time invariant.
Introducing the chemical potential μ as the partial molar free energy of a chemical species of a mixture with n species each one having N_i moles we have:

$$dG = -SdT + Vdp + \sum_{i=1}^{n} \mu_i dN_i$$

At thermal and mechanical equilibrium it reduces to:

$$dG = \sum_{i=1}^{n} \mu_i dN_i$$

Thus each of the μ_i of species i is explicitly defined as,

$$\mu_i = \frac{\partial G}{\partial N_i}\Bigg)_{T,P}$$

At phase equilibrium, the system Gibbs free energy reaches its minimum. It means,
$dG = 0$.
Which by the above definition gives,

$$\sum_{i=1}^{n} \mu_i dN_i = 0.$$

Considering a liquid vapor phase change situation,

$$\mu_L dN_L + \mu_g dN_g = 0$$

Mass conservation implies,

$$dN_l + dN_g = 0,$$

as the liquid and gas molar masses are equal.
Therefore,

$$\left(\mu_L - \mu_g\right) dN_L = 0$$

Close to equilibrium dN_L is small but non zero. The phase equilibrium condition consequently reads,

$$\mu_l = \mu_g .$$

Defining $g_k = \frac{\mu_k}{\hat{M}_k}$ it also reads,

$$g_L(p,T) = g_g(p,T).$$

Figures

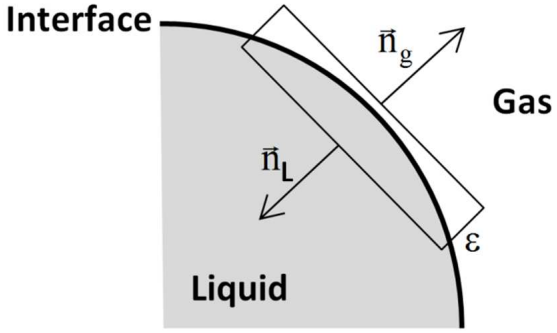

Figure 1. Schematic representation of a small control volume containing the interface.

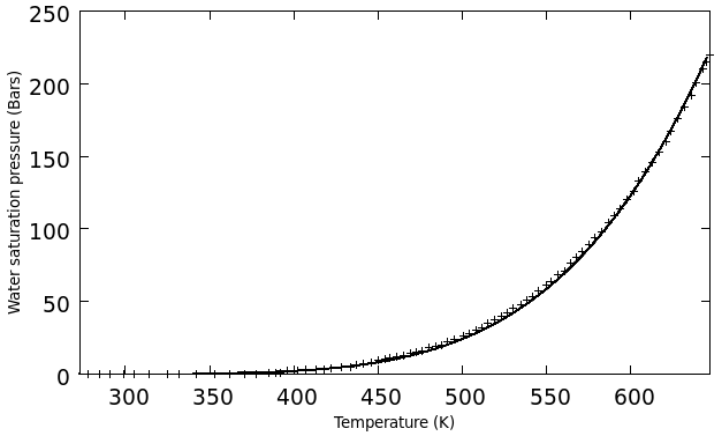

Figure 2. Comparison between the Rankine's formula adaptation (lines) and experimental data (symbols) showing excellent agreement.

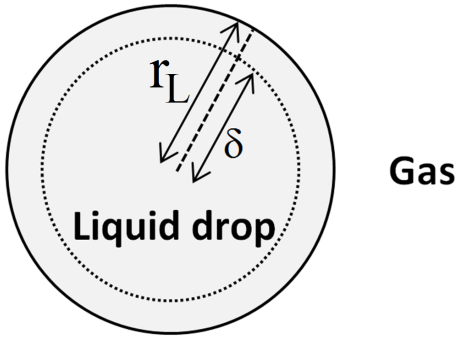

Figure 3 : Schematic representation of the liquid drop divided in two zones, a boundary layer of $r_L - \delta$ depth and a core zone of radius δ. In the boundary layer, the temperature has steep variations while it is assumed uniform in the core.

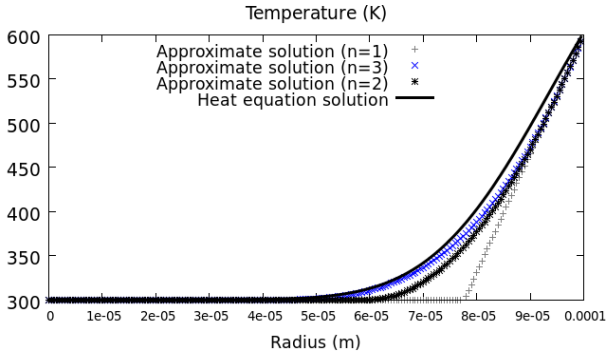

Figure 4: Short terms temperature profiles for different values of n. The dependence of the approximate solution to this parameter is not of minor importance.

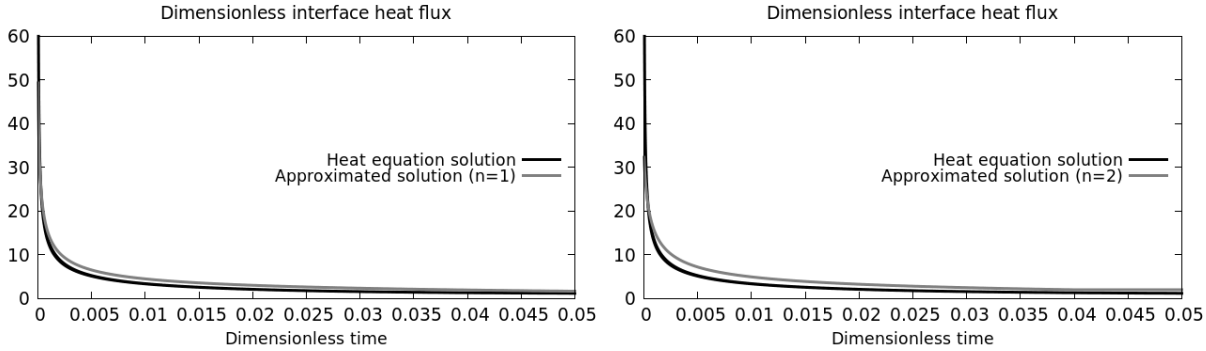

Figure 5: Dimensionless interface heat flux in gray lines for two values of n ($n=1$ on the left graph and $n=2$ on the right one) as a function of dimensionless time. These results are compared to the dimensionless heat equation solution (dark lines) showing very good agreement.

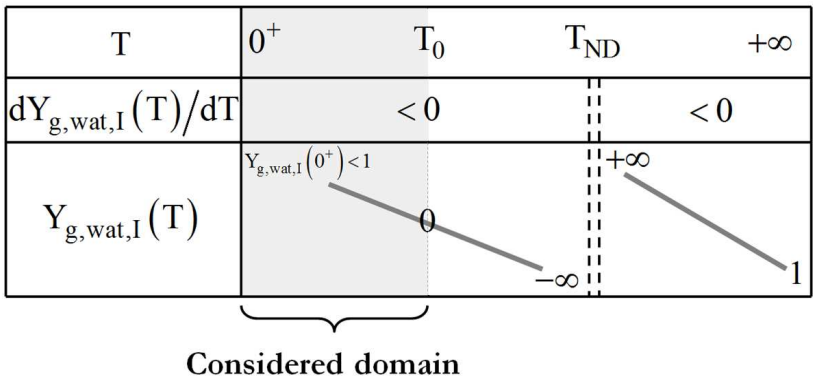

Figure 6: Mathematical analysis of function $Y_{g,wat,I}(T)$.

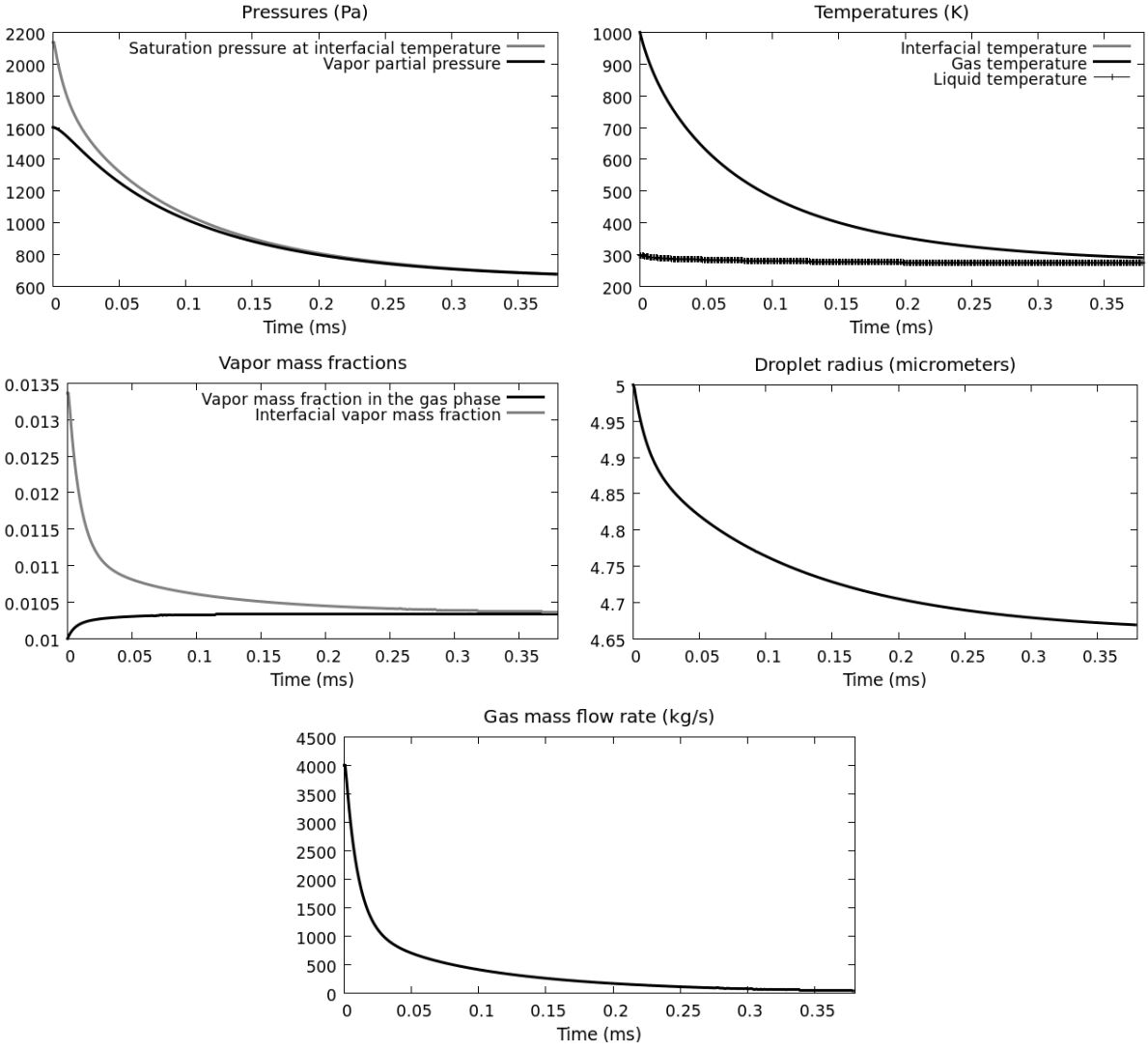

Figure 7: Evaporating droplets at rest. The equilibrium state is correctly reached at the end of the evaporation process.

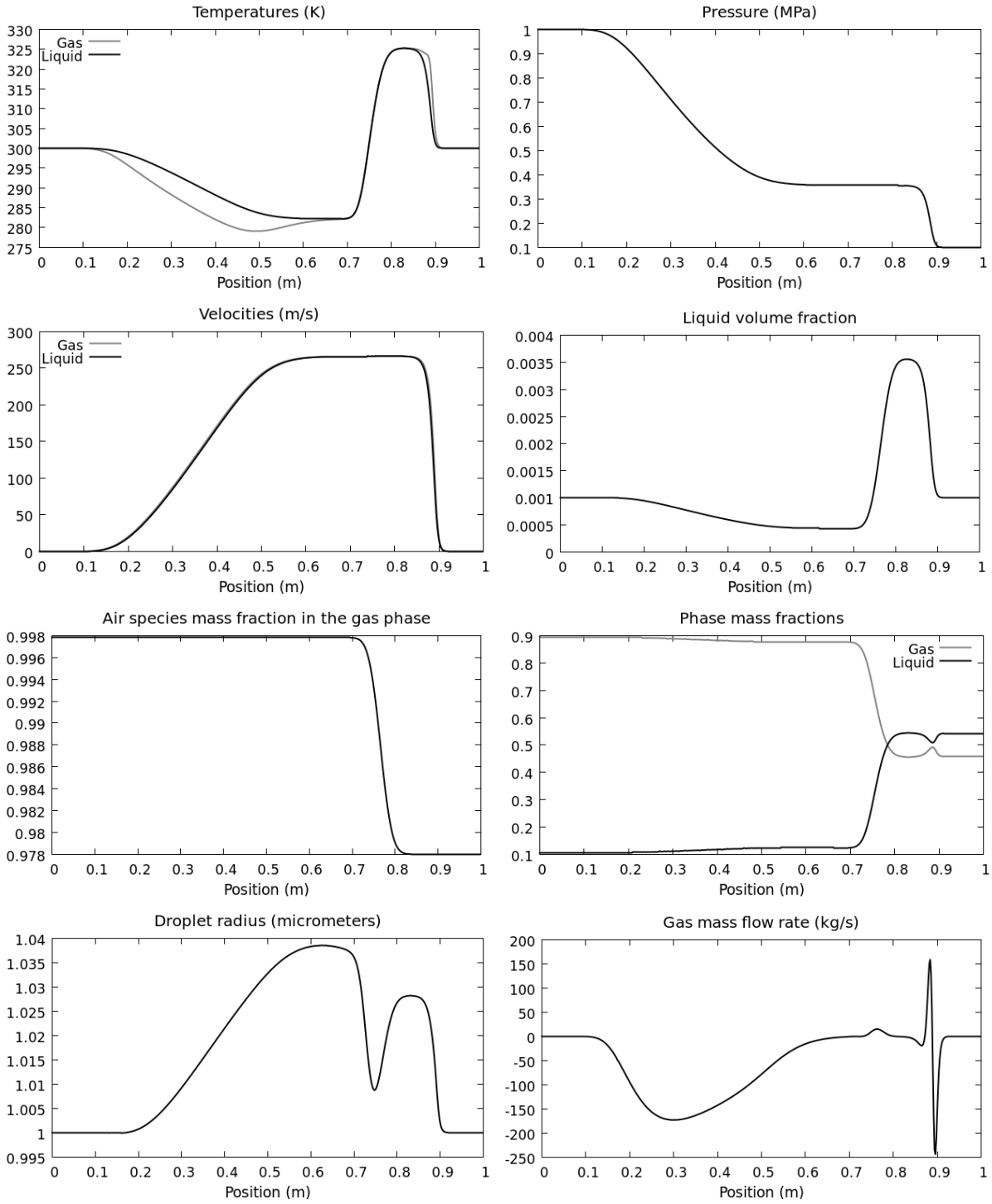

Figure 8: Gas-liquid shock with initial uniform volume fraction everywhere ($\alpha_g = 0.999$). The computations are made with drag effects and stiff pressure relaxation procedure, on a mesh involving 500 cells. The droplet radius is set to $1\mu m$. Results are shown at time $1ms$. Condensation occurs at most places.

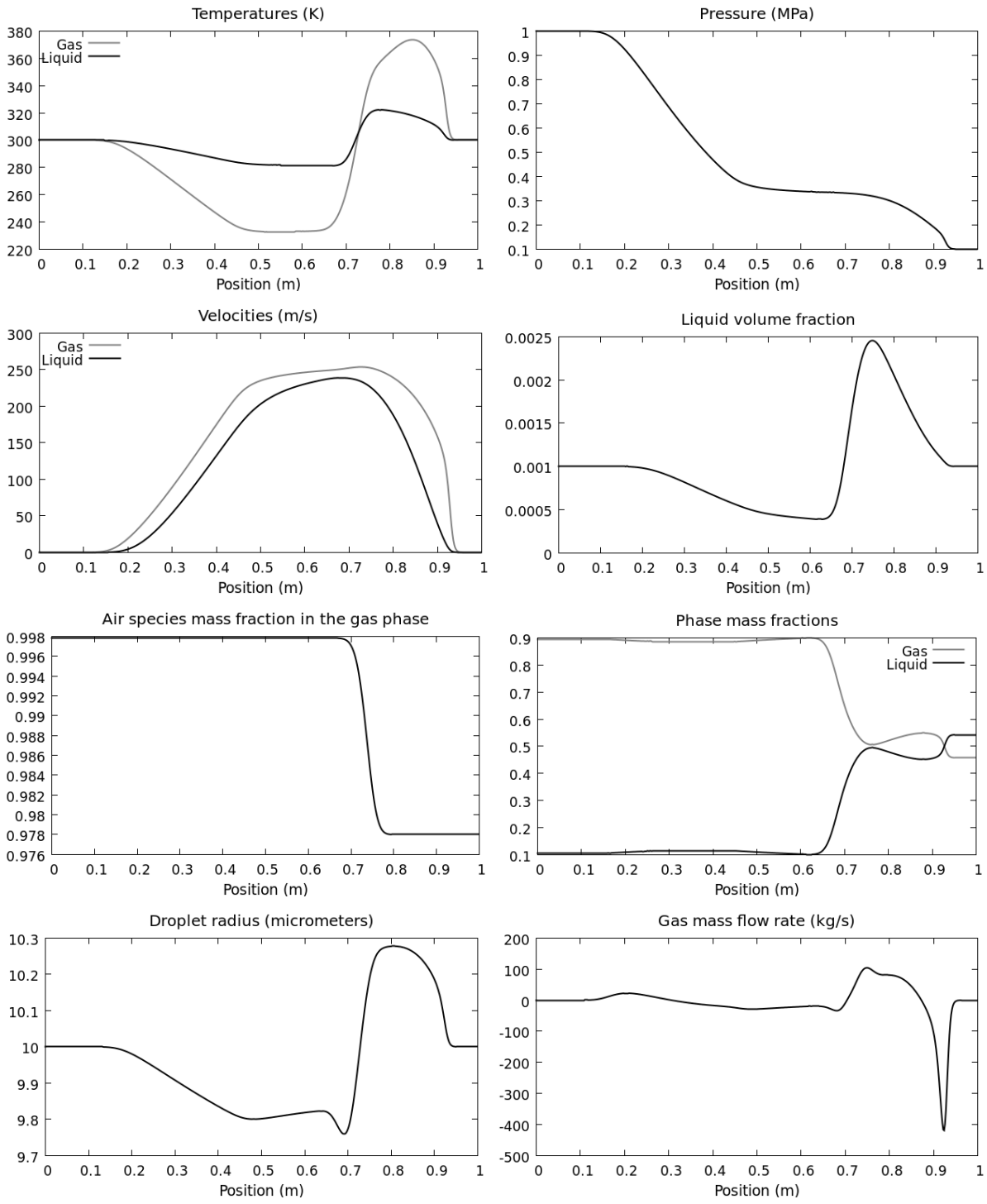

Figure 9: Shock tube containing gas and liquid phases with uniform volume fraction everywhere ($\alpha_g = 0.999$).The computations are made with drag effects and stiff pressure relaxation procedure, on a mesh involving 500 cells. The droplet radius is set to $10\mu m$. Results are shown at time $0.91ms$. Both condensation and evaporation are present.

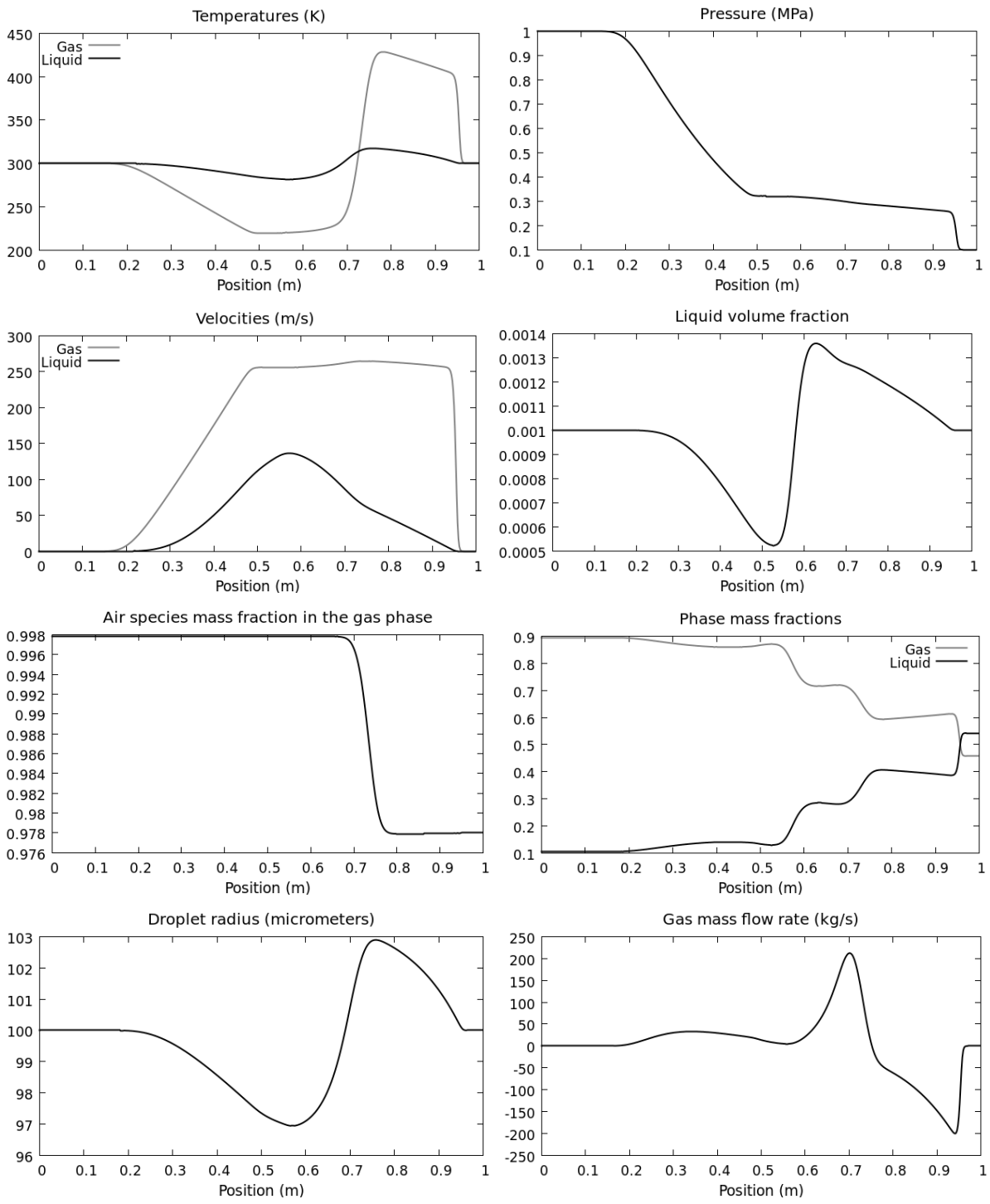

Figure 10: Shock tube containing gas and liquid phases with uniform volume fraction everywhere ($\alpha_g = 0.999$).The computations are made with drag effects and stiff pressure relaxation procedure, on a mesh involving 500 cells. The droplet radius is set to $100\mu m$. Results are shown at time $0.83ms$. Evaporation and condensation effects are enhanced.